Applied Energy 377 (2025) 124524

Contents lists available at ScienceDirect

Applied Energy

journal homepage: www.elsevier.com/locate/apenergy

Repurposing of supercritical coal plants into highly flexible grid storage with adapted 620 °C nitrate salt technology

Freerk Klasing *, Marco Prenzel, Thomas Bauer

German Aerospace Center, Institute of Engineering Thermodynamics, Linder Höhe, 51147 Cologne, Germany

HIGHLIGHTS

- Gas handling system elevates nitrate salt temperature limit up to 620 °C.
- Round-trip efficiency of up to 47.4 % for supercritical power plants.
- Up to 14 % cost savings with adapted 620 °C nitrate salt technology.
- Using a 620 °C single tank concept can reduce costs by 18 %.
- Molten salt system costs approximately 1/3 of lithium-ion battery costs.

GRAPHICAL ABSTRACT

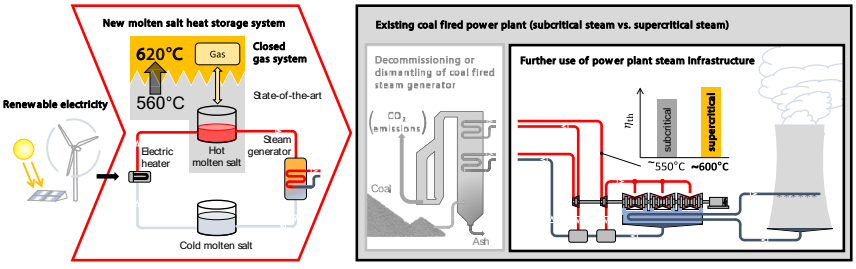

ARTICLE INFO

Keywords:
Long duration energy storage (LDES)
Molten salt (MS)
Grid-scale energy storage
Closed gas system
Techno-economic analysis
Concentrating solar power (CSP)
Carnot battery

ABSTRACT

Energy storage is essential for on-demand electricity generation from renewable sources like wind and photovoltaics. Repurposing fossil-fired power plants with thermal energy storage (TES) offers a cost-effective solution for large-scale grid energy storage. This paper explores converting supercritical coal plants into flexible grid storage systems using adapted nitrate salt technology. State of the art TES systems are limited by their maximum operating temperatures at up to 560 °C, but higher temperatures cause nitrate salts to decompose. Supercritical steam power plants require steam temperatures above 600 °C for optimal efficiency. To address this, a closed gas handling system can keep gaseous decomposition products within the nitrate storage system, stabilizing the salt at temperatures up to 620 °C.

This study presents the optimal design of such a gas system based on a techno-economic analysis and determines the overall electrical efficiency improvement of the supercritical power plant equipped with the adapted 620 °C storage compared to a subcritical power plant with 560 °C. The costs of repurposing power plants with two-tank and single-tank (thermocline) storage systems are evaluated, identifying potential cost savings of up to 18 % with the 620 °C single-tank system. The gas handling system costs are minimal. Compared to grid-scale lithium-ion batteries with a 10-h discharge duration, the levelized cost of storage (LCOS) for the proposed system is lower for low charging electricity costs. The 620 °C nitrate salt technology could further reduce LCOS in most cases worldwide.

This paper demonstrates the economic feasibility of a 620 °C molten salt system, highlighting cost savings over conventional options like batteries. The research provides valuable insights into repurposing existing fossil fuel infrastructure for a sustainable and efficient renewable energy transition.

* Corresponding author.
E-mail address: freerk.klasing@dlr.de (F. Klasing).

https://doi.org/10.1016/j.apenergy.2024.124524
Received 30 April 2024; Received in revised form 19 August 2024; Accepted 15 September 2024
Available online 23 September 2024

Nomenclature

Abbreviations

1T	Single-tank
2T	Two-tank
CAPEX	Capital expenditure
CF	Correction factor
cs	Cost share
CSP	Concentrating Solar Power
EH	Electric heater
eTES	Electro thermal energy storage
GHS	Gas handling system
LCOE	Levelized Cost of Electricity
LCOS	Levelized Cost of Storage
MS	Molten salt
rr	ramp rate
RT	Roundtrip
SG	Steam generator
TES	Thermal energy storage

Greek characters

Δ	difference, –
ρ	density, kg/m^3
η	Efficiency, –
σ	Stress, N/m^2

Latin characters

c	Specific cost, $€/kWh$, $€/kW$ *or* Specific heat capacity, J/kgK
C	Total costs, €
m	Mass, kg
n	Number of years, –
p	Pressure, bar
P	Power, W
Q	Thermal energy, J
r	Discount rate, –
t	Time, s
T	Temperature, $°C$, K
U	Heat transfer coefficient
V	Volume, m^3
W	Work, J

Subscripts

a	ambient
al	allowable
br	breathing gas
c	cold
ch	charge
circ	circulation
coal	coal fired power plant
com	compressor
comp	component
ct	cold tank
dc	discharge
dyn	dynamic
el	electrical
fd	foundation
g	gas phase
h	hot
ht	hot tank
ind	indirect
int	integration
loss	loss
net	net
nom	nominal
p	constant pressure
pr	process
real	real
ref	reference
s	salt phase
tank	tank
th	thermal

Superscripts

$\dot{}$	flow, 1/s

1. Introduction

The primary goal of the EU's Green Deal is to achieve climate neutrality by 2050. In order to achieve this political goal, the amount of installed capacity of renewable energy sources needs to be increased and the amount of fossil fired power generation needs to be ramped down [1]. To achieve net zero emissions by 2050 globally, the IEA estimated that it is required to triple the global installed capacity of renewable energy sources by 2030 and increase it ninefold by 2050 [2]. As the share of variable energy generation increases, there will be a significant need for energy storage systems with long storage duration to minimize curtailment, transmission, and grid flexibility requirements [3]. Thermal energy storage is a highly cost-effective option for storing large amounts of energy. The addition of components that convert electricity to thermal energy and back to electricity creates a system we call Carnot battery. However, there have been numerous other definitions for such a system in literature, e.g. thermal battery, electro-thermal energy storage (eTES), molten salt energy storage (MOSAS), thermal storage power plant (TSPP).

The distinctive feature of Carnot batteries is that their operational parameters align with those of batteries or pumped hydro storage. They can be charged with electricity and release electricity when discharged.

The first work on Carnot batteries dates back to 1924, when Marguerre proposed a combination of mechanical and thermal energy storage for storing electricity by means of steam compression, a rankine-cycle and steam accumulators. The first concept using only thermal energy storage for storing electricity was presented by Cahn et al. in 1978 [4,5]. Since then, there have been a number of studies on thermal energy storage (TES) in concentrated solar power (CSP) [6–8], coal fired power plants [9–14] and standalone Carnot batteries [5,15–18] intended for the green field. Other concepts include retrofitting existing thermal power plants with electrically charged TES [19,20] or proposing the integration of TES into the steam infrastructure of chemical sites or combined heat and power [21–24]. It was also recently announced that a 560 MW coal-fired power plant in Chile is to be retrofitted with a 10 h, 560 °C molten salt storage system [25,26].

This retrofitting concept requires a molten salt system consisting of an electric heater, a hot and a cold tank and a steam generator as shown in Fig. 1. The benefits of using molten salt as a storage medium include the ability to use non-pressurized large tanks and the dual function of molten salt as both a storage medium and a heat transfer fluid (HTF). This dual functionality eliminates the need for an additional heat exchanger, unlike parabolic trough systems that use synthetic oil as HTF. Additionally, nitrate molten salt is non-toxic and non-flammable. Solar Salt, composed of 60 wt% sodium nitrate and 40 wt% potassium nitrate, solidifies at approximately 223 °C [27]. To maintain the liquid state of the salt, electric trace heating is required for pipes and equipment to prevent solidification, especially when there is no salt flow and the pipes are not drained. A state-of-the-art 560 °C molten salt storage system is sufficient for retrofitting subcritical steam power plants with temperatures of approximately 550 °C. For higher temperatures, technologies

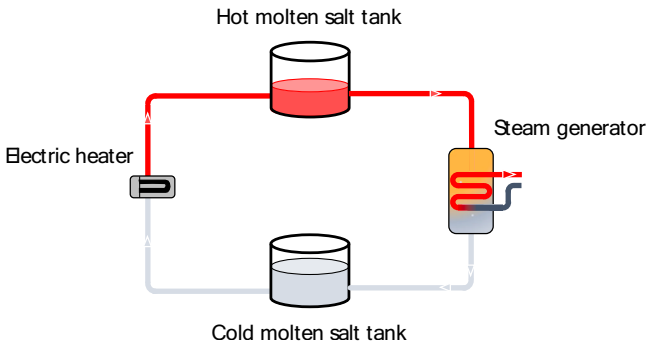

Fig. 1. Illustration of molten salt storage system for retrofitting concept.

like alumina packed beds (700 °C), chloride salts (800 °C), solid particles (1000 °C), liquid silicon (2000 °C) and graphite (2400 °C) have been proposed [28–31]. Although these are innovative approaches, the technologies are yet to be demonstrated in a larger scale. Nitrate salt storage remains the commercially most employed grid connected thermal energy storage, with a total of 491 GWh of installed capacity globally as of today [32]. Unlike other storage media, adapting nitrate salt technology does not require the development of an entirely new large-scale storage system, but only small additions have to be made. Therefore, we propose an enhanced nitrate salt technology incorporating an active gas handling system. This system can increase the current temperature limit from 560 °C to 620 °C by decreasing corrosive attack. In this way the higher steam parameters of a supercritical power plant of approximately 600 °C can be met.

The main advantage of choosing supercritical over subcritical cycles is seen in the much higher efficiency: e.g. Mancini et al. indicate an efficiency increase of up to 13 % for CSP [33]. One reason why this technology has not been realized yet, is because of salt instability above 560 °C: Raising the temperature of the nitrate salt above 560 °C in an air atmosphere accelerates the decomposition of the salt, ultimately forming corrosive oxides in the molten salt. Controlling the gas atmosphere in the salt tanks can limit salt decomposition and corrosion to an acceptable level. Experiments from Bonk et al. presented clear evidence of the enhanced thermal stability of solar salt in long-term by using a closed gas atmosphere [34]. Experiments from Sötz et al. and Steinbrecher et al. support these findings by demonstrating stable oxide-ion contents, as an indicator for corrosivity, after 1000 h and even regeneration of decomposed solar salt by adding small amounts of nitrous gases to the purge gas [35–37]. Subsequent investigations into the impact of elevated salt temperatures on corrosion were conducted by Bonk et al. [38,39]. Their findings revealed that for the austenitic steel 347H, a material commonly utilized for the hot tank of molten salt storage, corrosion in Solar Salt is markedly influenced by temperature and the composition of the cover gas. Fig. 2 illustrates this effect for 570 °C with synthetic air cover gas and 620 °C with either synthetic air cover gas or a reactive gas composed of 80 % oxygen and 400 ppm NO. As can be observed, the corrosion rate at 620 °C with reactive cover gas is only marginally higher than the corrosion rate at 570 °C, whereas the corrosion rate at 620 °C with synthetic air cover gas is approximately three times as high.

The stabilizing effect can be attributed to the fact that the decomposition of nitrate salts can be regarded as an equilibrium reaction that occurs in both directions. The decomposition of nitrate salts occurs in two stages. In a first step the nitrate ion reacts to oxygen and a nitrite ion:

$$NO_3^- \rightleftharpoons 0.5O_2 + NO_2^- \quad (1)$$

In a second step the nitrite ion further reacts to an oxide ion and nitrous gases:

$$2NO_2^- \rightleftharpoons O^{2-} + NO + NO_2 \quad (2)$$

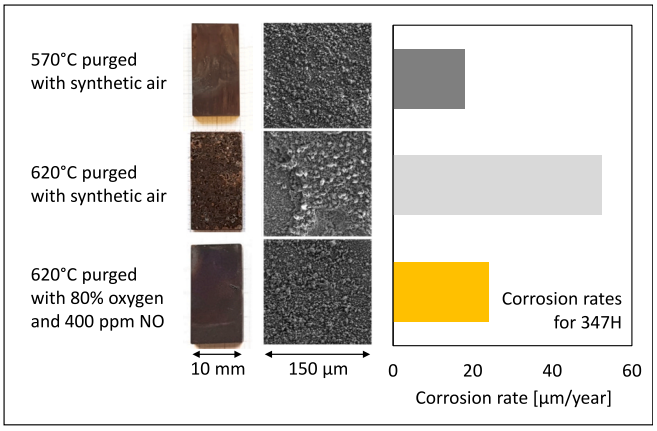

Fig. 2. Effect of temperature and cover gas composition on corrosion of 347H in Solar Salt. Surface image and corrosion rate after 1000 h of testing, redrawn from [39].

Although an increased nitrite ion content is not critical, an increased oxide ion content has a negative impact on the corrosivity of the salt. The equilibrium shifts to the right in both reactions with increasing temperature. However, increasing the partial pressure of the reaction gases shifts the equilibrium back to the left. In state-of-the-art two-tank storage applications, the gas atmosphere in the tanks constantly exchanges gas with the ambient air, keeping the partial pressure of oxygen and nitrous gases low. To equilibrate the partial pressures of the reaction gases at a higher level, the system can be closed, leading to higher partial pressures of oxygen and nitrous gases after an initial production of oxygen and nitrous gases. The stabilizing effect of closing the system has been demonstrated by Kunkel et al., who showed that salt stability could be maintained at a scale of 100 kg at a temperature of 620 °C for over 3500 h [40].

However, restricting the free expansion of salt and gas poses a challenge due to the potential pressure buildup in the tanks. Typically, large flat-bottom tanks are designed to withstand a maximum overpressure of approximately 170 mbar [41]. For higher pressures, alterations to the tank shape should be considered, with a view to adopting a more spherical design, as is the case with pressure vessels. The current designs of pressure vessels have a maximum capacity of approximately 100 to 500 cubic meters, due to the fact that they are factory-built [42]. A 1000 MWh molten salt storage system, however, necessitates a volume exceeding 5000 cubic meters. Consequently, a redesign comprising multiple smaller pressure vessels is inadvisable, given the considerable increase in costs that would be incurred.

Therefore, in this work, we propose a closed gas handling system (GHS) that actively controls the pressure in the tanks, allowing the tanks to be designed at atmospheric pressure levels. Limiting the design pressure is a prerequisite for this concept. The volume of recurrently contracting and expanding gas must be collected in a separate container, in this case a pressure vessel.

The benefit of focusing on supercritical steam parameters is that higher thermal efficiencies can be achieved with this type of power plants. The paper examines the total component costs and electrical-to-electrical efficiencies, also known as roundtrip efficiency (η_{RT}), of the retrofitted parts of the 560 °C versus 620 °C concept. This includes a newly introduced gas system for the latter.

The authors expect further cost reduction potential from the use of a single-tank (1T) storage system instead of a two-tank storage system (2T). The single-tank concept is based on the principle of separating two liquid volumes with different buoyancies due to their varying densities at different temperatures. In this concept the hot molten salt floats at the top, while the cold molten salt is at the bottom. Between these two volumes, there is a temperature transition zone also called thermocline. Experiments conducted in a 2.2-m diameter tank demonstrated that a

thermocline thickness of less than one meter could be observed at temperatures ranging from 290 °C to 550 °C for this concept [43]. Although this was for a 24-h duration, the thermocline thickness in a real system depends markedly on how the storage is operated. The temperature profile is shaped by external operating conditions. Since the thermocline expands over time due to convective mixing [44] and heat conduction, it is essential to periodically extract this zone from the storage tank, at least partially. This practice maintains the stratification's compactness and minimizes the amount of salt at an unusable intermediate temperature. Extracting the thermocline zone is crucial for preserving its compactness [45–47]. During the end of a charging or discharging process, the temperature of the returning liquid from the storage rises or falls, respectively. The further the storage is charged or discharged, the steeper the temperature profile becomes in the next cycle. While there are various methods for constructing such a tank, including a packed bed, encapsulated phase change material (PCM) or a moving barrier, the simplest approach appears to be a single tank with no filler material or moving barrier. Especially for the elevated temperature of 620 °C there are open research questions regarding filler salt interaction leading to salt degradation and thermal ratcheting. For these reasons in this study we propose to use a single-tank storage with no additional filler material.

A technoeconomic analysis was conducted to compare a 620 °C molten salt thermal energy storage (2T and 1T) integrated into an existing supercritical power plant with a 560 °C molten salt storage system and grid-scale lithium-ion batteries.

The originality and novelty of this work is a new method for energy storage by retrofitting existing fossil-fired power plants with thermal energy storage (TES) systems that use nitrate salt up to 620 °C. The proposed closed gas system prevents the decomposition of nitrate salts at elevated temperatures. This innovative approach addresses a critical gap in current storage technology and enables the retrofitting of supercritical power plants into Carnot batteries. The study presents a comprehensive techno-economic analysis, which reveals potential cost savings and improved efficiencies compared to state-of-the-art solutions using molten salt. The gas handling system (GHS) is optimized to integrate molten salt storage systems into supercritical power plants, resulting in the highest efficiencies.

The presented work is relevant for large-scale grid energy storage integration, which is crucial for the deployment of renewable energy. It compares and highlights the cost-effectiveness and longevity of this approach and lithium-ion battery systems. Furthermore, this work presents an analysis of the technical and economic competitiveness of converted supercritical coal-fired power plants that use molten salt storage. The literature on techno-economic issues related to high-temperature storage in coal-fired power plants assumes a maximum operating temperature of approximately 560 °C for salt storage.

To date, no one in the CSP or any other sector has demonstrated molten nitrate salt stability at an elevated temperature of 620 °C on a large scale. A gas handling system is considered to be a crucial component for the widespread implementation of 620 °C nitrate salt technology, even beyond CSP. This concept is a new approach with significant potential in the context of repurposing coal-fired power plants using molten salt thermal energy storage.

2. Method

2.1. Assumptions and description of a closed gas handling system for the 620 °C concept

A closed GHS is required to compensate for volume expansion in the tank system and to prevent gas exchange with the atmosphere. Fig. 3 shows a schematic diagram of a GHS in gas storage mode (dark grey) and gas release mode (pale grey). The GHS consists of a pre-cooler, a gas compressor with motor, an after-cooler, a pressure vessel as well as a control valve and an electric heater. A pressure control unit controls the gas flow to and from the pressure vessel.

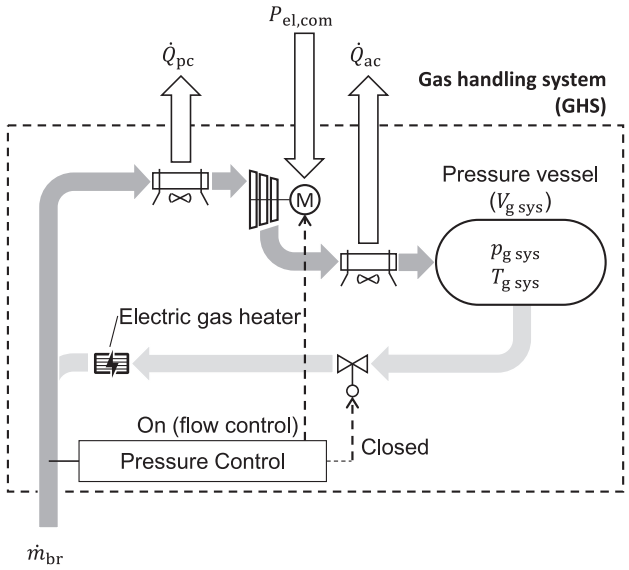

Fig. 3. Schematic diagram of a GHS in gas storage mode (marked by dark grey, inactive parts are pale grey).

In **gas release mode** ($p_{storage} < p_{atm}$), gas is released from the pressure vessel via the control valve to compensate for the slight negative pressure in the storage system (a few mbar). The gas temperature can be raised with the electric heater to avoid local salt solidification when entering the storage system.

In **gas storage mode** ($p_{storage} > p_{atm}$), gas is pumped from the storage system via a controlled compressor into the pressure vessel to compensate for the slight overpressure that develops as a result of temperature change in the storage system. The gas is selectively cooled to ambient temperature by means of a pre-cooler and an after-cooler (upstream and downstream of the compressor). It is assumed that the compressor operates at 50 °C inlet temperature.

As already described, the filling level of the two-tank storage system changes in each tank during charging and discharging. As a result, gas above the molten salt is either pushed out or has to flow in so that the pressure is completely equalized with the atmosphere as flat bottom tanks operate close to atmospheric pressure conditions (mbar range) due to static reasons. In the two-tank storage system, the gas flows from one tank to the other via a so-called gas balance line. Fig. 4 illustrates the heat and mass flows during discharging of a two-tank storage system. In this process, the balance gas undergoes a temperature change. This results in additional gas expansion or contraction, so that additional gas is supplied to or excess gas escapes from the storage system. In the case of the state-of-the-art two-tank storage system, this process is also referred to as “tank breathing” because the air exchange takes place directly with the atmosphere. At elevated storage temperatures where a closed gas system is required, the excess of breathing air mass flow must be compensated by the GHS. The mass flows can be determined using a mass and energy balance as a function of the heat input and output to the salt.

During the discharge of the two-tank storage system, molten salt is pumped from the hot tank through a heat exchanger, where it is cooled down and transferred to the cold tank. This change in temperature leads to a contraction of the salt, which ultimately increases the total gas volume in the two tanks. Concurrently, cold gas is flowing from the cold tank through the connecting gas balance line to the hot tank. In the hot tank, the entering cold gas is immediately heated by the large thermal mass of the hot tank and expands as it is an isobaric process. The gas expansion is greater than the molten salt contraction, resulting in an excess of gas, which we refer to as breathing gas. Consequently, during

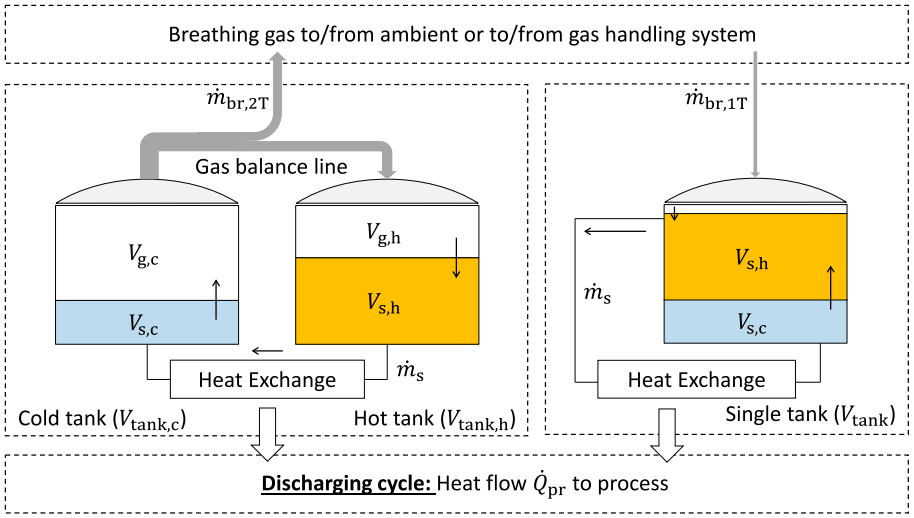

Fig. 4. Schematic illustration of the heat and mass flows during discharging for a two-tank (left) and a single-tank system (right).

discharging, the two-tank storage system "breathes out". During charging it "breathes in". In a single-tank system, the gas phase remains at a constant temperature, while the molten salt undergoes a temperature change. Consequently, the amount of breathing gas is solely determined by the molten salt expansion and contraction. As a result, $\dot{m}_{br,1T}$ is lower than $\dot{m}_{br,2T}$ and flows in the opposite direction.

Under the assumption of a constant specific heat capacity $c_{p,s,ref}$ of the salt, a mass and energy balance over the two tanks (system limit indicated with dashed lines in Fig. 4) yields the following gas mass flow $\dot{m}_{br,2T/1T}$ as a function of the heat flow $\dot{Q}_{pr}$ that is supplied or removed in the process, the temperatures T_{hot} and T_{cold}, and the densities $\rho_{g,c}$, $\rho_{g,h}$, $\rho_{s,c}$, and $\rho_{s,h}$:

$$\dot{m}_{br,2T} = \dot{Q}_{pr} \cdot \left(\rho_{g,c}/\rho_{s,c} - \rho_{g,h}/\rho_{s,h}\right) / \left(c_{p,s,ref} \cdot (T_h - T_c)\right) \quad (3)$$

$$\dot{m}_{br,1T} = -\dot{Q}_{pr} \cdot \left(\rho_{g,h}/\rho_{s,c} - \rho_{g,h}/\rho_{s,h}\right) / \left(c_{p,s,ref} \cdot (T_h - T_c)\right) \quad (4)$$

The total volume of gas at atmospheric pressure and ambient temperature T_{amb} during a breathing cycle ($V_{br,a,2T/1T}$) can be expressed as a function of the volume of salt available for heat storage $V_{s,c}$ and the temperature-dependent densities of salt and gas ($\rho_{g,a}$, $\rho_{g,c}$, $\rho_{g,h}$, $\rho_{s,c}$, and $\rho_{s,h}$) for both two-tank storage and single-tank storage. The primary distinction between two-tank and single-tank storage is that in the former, approximately 50 % of the storage volume is consistently occupied by gas. The fluctuating liquid level of the two tanks necessitates the flow of gas from one tank to the other. This process of gas balancing is associated with a change in the temperature of the gas, which in turn results in a change in the volume of the gas. As an illustration, the breathing gas volume for a molten salt two-tank storage system (620 °C hot tank and 290 °C cold tank temperature) can be evaluated. This results in a breathing gas volume at ambient temperature and pressure that is approximately 15 % of the volume of the salt at the cold tank temperature. In contrast, for the single-tank storage system, this ratio is only 4 % at the same conditions.

$$V_{br,a,2T} = V_{s,c} \cdot \left(\rho_{g,c}/\rho_{g,a} - \left(\rho_{s,c} \cdot \rho_{g,h}\right) / \left(\rho_{s,h} \cdot \rho_{g,a}\right)\right) \quad (5)$$

$$V_{br,a,1T} = -V_{s,c} \cdot \left(\rho_{g,h}/\rho_{g,a} - \left(\rho_{s,c} \cdot \rho_{g,h}\right) / \left(\rho_{s,h} \cdot \rho_{g,a}\right)\right) \quad (6)$$

The heat loss $Q_{loss,br,2T/1T}$ that occurs due to "breathing" during one complete charge and discharge cycle is obtained by an energy balance and integration. It can be expressed in terms of the specific heat of the gas $c_{p,g,ref}$, salt temperatures T_h, T_c and temperature of the gas entering the tank $T_{br,in}$, densities $\rho_{g,c}$, $\rho_{g,h}$, $\rho_{s,c}$, and $\rho_{s,h}$ as well as the utilized salt mass m_s. In accordance with the aforementioned example, the total heat loss during a single cycle would then amount to a mere 0.006 % (2T) or 0.003 % (1T) of the total heat stored within the storage system.

$$Q_{loss,br,2T} = c_{p,g,ref} \cdot \left(T_c - T_{br,in}\right) \cdot \left(\rho_{g,c}/\rho_{s,c} - \rho_{g,h}/\rho_{s,h}\right) \cdot m_s \quad (7)$$

$$Q_{loss,br,1T} = -c_{p,g,ref} \cdot \left(T_h - T_{br,in}\right) \cdot \left(\rho_{g,h}/\rho_{s,c} - \rho_{g,h}/\rho_{s,h}\right) \cdot m_s \quad (8)$$

2.2. Cost assumptions for the molten salt heat storage system

Cost estimation was performed using available data from the literature as well as physical relationships introducing correction factors *CF*. Exact values of the introduced correction factors are presented in the result and discussion section.

For the cost calculation of the two-tank storage system, total specific TES costs ($c_{2T,ref}$) of 21 €/kWh related to the energy content were assumed [48]. For the state of the art, Glatzmeier et al. gives the following cost shares of the total costs of the storage system listed in Table 1 [49].

An increase in the operating temperature from 560 °C to 620 °C has the effect of both increasing the mechanical strength requirements of the hot tank and enhancing the energy density of the storage system. This is due to the fact that as the temperature difference is increased, it becomes possible to store more energy in the same amount of salt. Both phenomena are reflected in the specific costs c_{2T} with the aid of two temperature-dependent correction factors, *CF*1 for the energy density and *CF*2 for the mechanical strength.

$$c_{2T} = CF1 \cdot CF2 \cdot c_{2T,ref} \quad (9)$$

The costs of single-tank storage differ from those for two-tank storage in that the cost of a cold tank and the associated tank supports, foundations and site work are not required. This is described by the factor *CF*3. There are also costs for additional salt and larger sizing of the tank due to the thermocline zone. This is described by the factor *CF*4. In addition, slightly higher wall thicknesses are required to accommodate for additional bending stresses induced by the temperature profile. This

Table 1
Cost share for a molten salt storage system based on Glatzmeier et al. [49].

Description of cost share	Variable name	Value
Hot tank including pump	cs_{ht}	27 %
Cold tank including pump	cs_{ct}	12 %
Salt	cs_s	46 %
Tank supports, foundations and site work	cs_{fd}	10 %
Electrical, instrumentation, piping, valves and fittings	–	5 %

is described by the factor *CF*5. Scaling constraints due to other thermal stresses were neglected in this study. Therefore, the results must be handled with care:

$$c_{1T} = CF1 \cdot CF2 \cdot CF3 \cdot CF4 \cdot CF5 \cdot c_{2T,ref} \quad (10)$$

For the state-of-the-art salt electric heater, a constant specific cost ($c_{EH,ref}$) of 100 €/kW was assumed [19]. However, as the temperature increases, the heat flux in the heating elements decreases. Therefore, in this study, a one-dimensional model for the electric heater was developed solving first principle equations in Matlab. It was assumed, that all fluid properties where independent from temperature and therefore constant. On this basis the correction factor *CF*6 was evaluated as a function of the inlet and outlet temperature. The specific cost of the electric heater can thus be calculated as follows:

$$c_{EH} = CF6 \cdot c_{EH,ref} \quad (11)$$

The molten salt steam generator of a subcritical steam cycle usually consists of at least four heat exchangers (preheater, evaporator, superheater and reheater) and a steam drum with forced circulation. A constant specific cost ($c_{SG,ref}$) of 46 €/kW [48] was assumed for the subcritical steam generator. A supercritical molten salt steam generator was assumed to be built as a once-through steam generator consisting of one single heat exchanger per pressure level. The transition from a subcritical molten salt steam generator $c_{SG,560°C}$ to a supercritical steam generator $c_{SG,620°C}$ can be denoted as:

$$c_{SG,560°C} = CF7 \cdot c_{SG,ref} \quad (12)$$

$$c_{SG,620°C} = CF8 \cdot c_{SG,560°C} \quad (13)$$

The correction factor *CF*7 represents the cost deviation due to a pinch point variation. Steam parameters for the reference steam generator were based on an IEA report from 2007 [50]. The correction factor *CF*8 comprises for the effect of different materials, wall thicknesses and steam generator layouts for supercritical steam generators due to the temperature increase.

The specific cost for the GHS $c_{GHS}[€/kWh]$ related to the thermal storage capacity (Q_{th}) was estimated based on the costs for the components pressure vessel, compressor, air cooler, electric heater, and balance of plant. The specific cost of the GHS can be calculated as follows, where C_Y represents the total component costs of each component Y:

$$c_{GHS} = \sum C_Y \Big/ Q_{th} \quad (14)$$

The following assumptions for C_Y listed in Table 2 were made.

2.3. Efficiency definitions

A range for the net efficiency of sub- and supercritical coal fired power plants is presented in [50]. A range for the thermal efficiency of the power plant can be calculated using following formula, where $\eta_{net,coal}$ is the nameplate net efficiency of the coal fired power plant, $\eta_{SG,coal}$ and $\eta_{SG,s}$ are the efficiencies of the coal and salt steam generators and $\eta_{net,s}$ is the net efficiency of the of the repurposed power plant (heat from molten salt storage to electricity).

$$\eta_{net,s} \approx \eta_{net,coal} \cdot \eta_{SG,s} / \eta_{SG,coal} \quad (15)$$

A range for the so-called nominal round-trip-efficiency of a repurposed power plant can be calculated by multiplying the subcomponent efficiencies of the steam generator, the electric heater, the thermal energy storage and the power plant:

$$\eta_{RT,nom} \approx \eta_{EH} \cdot \eta_{TES} \cdot \eta_{net,s} \quad (16)$$

As conventional coal-fired power plants are mostly designed for continuous power supply, the repurposed options with a TES will most likely be used with one or two daily cycles, requiring steep ramp rates so that it can be used like a 'grid connected battery'. The startup times of conventional coal-fired power plants depend on how long the power plant has been shut down before [55]. A plant starting from a completely cold state can take several hours to reach full capacity. For this reason, a new efficiency η_{dyn} considers the need to dump power from the plant that cannot be ramped down fast enough or needs to be ramped up well in advance (warm or cold start-up).

$$\eta_{RT,real} \approx \eta_{dyn} \cdot \eta_{RT,nom} \quad (17)$$

An exemplary load profile and the corresponding generator and electric heater load for a storage powerplant is displayed in Fig. 5. The ramp rate *rr* is defined as the normalized maximum achievable power increase or decrease per time:

$$rr = |\partial P_{el} / \partial t|_{max} \cdot 1 / P_{el,nom} \quad (18)$$

The energy demand for charging $W_{el,ch}$ and the energy amount transferred during recycling $W_{el,circ}$ can be calculated as follows:

$$W_{el,ch} = \left(W_{el,dc} + W_{el,circ}\right) / \eta_{RT,nom} - W_{el,circ} \quad (19)$$

$$W_{el,circ} = \left(P_{el,nom} + P_{el,min}\right) / rr \quad (20)$$

According to Fig. 5 the dynamic efficiency η_{dyn} can be calculated as follows:

$$\eta_{dyn} = t_{dc} / \left(t_{dc} + \left(1 + P_{el,min} / P_{el,nom}\right) / rr \cdot \left(1 - \eta_{RT,nom}\right)\right) \quad (21)$$

Table 2
Assumed component costs C_Y of gas handling system in 2023.

Component Y	Cost function for 2023 in € (C_Y)	Variable *X*	Notes	Ref.
Pressure vessel	$11 \cdot X$	Mass of steel, *kg*	Wall thickness according to [51], minimum wall thickness 20 mm	[42]
Compressor	$2035 \cdot (10 \cdot X)^{0.6}$	Power, *kW*	Carbon steel	[52]
Air-Cooler	$194 \cdot X + 19319$	Heat transfer area, m^2	$U = 15\ W/m^2K$	[53]
Electric Gas Heater	$218 \cdot X$	Power, *kW*		[54]
Balance of plant*	$0.49 \cdot X$	Total component costs, €	Gas processes '$\leq 400\ ^\circ F$'	[53]

* Balance of plant includes: foundation, structural steel, buildings, insulation, instrumentation, electrical, piping, painting and miscellaneous.

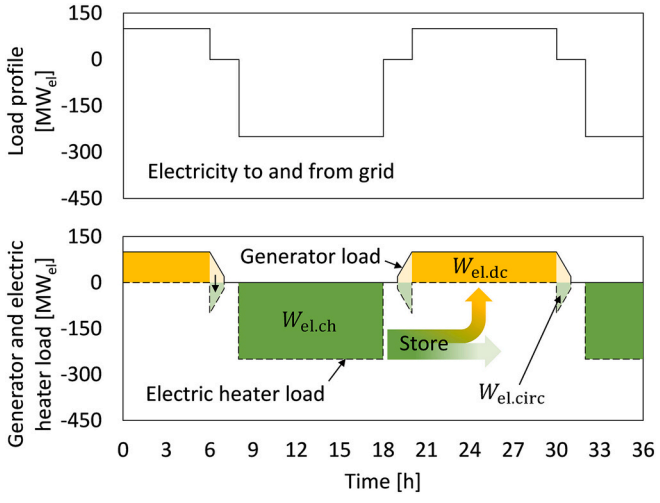

Fig. 5. Load profile (top) and generator and electric heater load (bottom) for a time period of 36 h and a charge and discharge time of 10 h with 2 h of zero electricity production.

2.4. Levelized cost of storage

According to Jülch et al. [56] the levelized cost of storage (LCOS) is defined as the discounted cost per unit of discharged electricity for a specific storage technology and application. It can be expressed as follows:

$$\mathrm{LCOS} = \frac{\mathrm{CAPEX} + \sum_n^N \frac{\text{O\&M cost}}{(1+r)^n} + \sum_n^N \frac{\text{Charging cost}}{(1+r)^n} + \frac{\text{End of life cost}}{(1+r)^{N+1}}}{\sum_n^N \frac{W_{\mathrm{el,dc}}}{(1+r)^n}} \quad (22)$$

With CAPEX being the capital expenditure of a project or system, O&M cost containing all costs related to operation and maintenance during one year of operation, Charging cost expressing the electricity cost for charging and End of life cost being the costs that are related to decommissioning of the plant. The variable r is the interest rate and $W_{\mathrm{el,dc}}$ is the amount of electricity produced during one year.

CAPEX includes the costs of the major components $\mathrm{CAPEX_{comp}}$ (comprising electric heater, storage tanks and steam generator) as well as the costs for associated integration efforts $\mathrm{CAPEX_{int}}$ (comprising piping, instrumentation, civil and electrical integration) and indirect costs $\mathrm{CAPEX_{ind}}$.

$$\mathrm{CAPEX} = \mathrm{CAPEX_{comp}} + \mathrm{CAPEX_{int}} + \mathrm{CAPEX_{ind}} \quad (23)$$

The indirect costs $\mathrm{CAPEX_{ind}}$ were assumed proportionally to the component costs $\mathrm{CAPEX_{comp}}$, which can be calculated from the specific component costs described in the section 2.2, the charge and discharge duration t_{ch} and t_{dc}, the net efficiency of the repurposed power plant $\eta_{\mathrm{net,s}}$ as well as the nominal electric capacity of the plant P_{el}.

$$\mathrm{CAPEX_{comp}} = P_{\mathrm{el}} \cdot \left(\left(c_{\mathrm{2T;1T}} + c_{\mathrm{GHS}} \right) \cdot t_{\mathrm{dc}} + c_{\mathrm{EH}} \cdot t_{\mathrm{dc}} / t_{\mathrm{ch}} + c_{\mathrm{SG}} \right) / \eta_{\mathrm{net,s}} \quad (24)$$

As all specific component costs are a function of the cold tank temperature T_{c}, optimization was required to determine the lowest value for the total costs $\mathrm{CAPEX_{comp}}$. The optimized cases were then used for the cost calculation.

A margin of +/− 20 % uncertainty of the total CAPEX was assumed for this approach. This paper neglects the end-of-life costs, which is a common approach [56]. Fig. 6 illustrates the overall methodology of LCOS-calculation, which is based on three pillars:

1. Financial parameters (e.g. interest rate r and timespan N) and operating and maintenance (O&M) costs
2. The minimum and maximum values for the round-trip efficiency for the two investigated repurposing options MS-560 and MS-620
3. The investment costs for repurposing projects which are calculated based on the required component size.

In order to size the components, it is necessary to know the round-trip efficiency and to define the electrical power, charging and discharging duration. In this study, a constant capacity of 100 $\mathrm{MW_{el}}$ is assumed, with a charging and discharging duration of 10 h each. The specific component costs for the MS-560 system are based on values from literature, while for the MS-620 system, the introduced correction factors were used. The correction factors are based on physical relationships or referenced techno-economic investigations.

3. Results

3.1. Comparison of round-trip-efficiencies of retrofitted thermal power plants

Worldwide built supercritical coal-fired power plants (lignite and hard coal) have on average 9 % higher net efficiencies than built subcritical plants [50]. An approximate range for the net electrical efficiency of subcritical and supercritical coal-fired power plants ($\eta_{\mathrm{net,coal}}$) and the steam generator efficiency (η_{SG}) is given in Table 3. The two newly introduced repurposing options **MS-560** and **MS-620** are also evaluated here in terms of their sub-component efficiencies. The option MS-560 is a state-of-the art molten salt storage system, the option MS-620 is an advanced molten salt storage system with elevated temperature and a GHS and with an 2T or 1T storage system. On the basis of these sub-component efficiencies, a range for the expected nominal round-trip-efficiency ($\eta_{\mathrm{RT,nom}}$) for the options MS-560 and MS-620 was calculated. The different losses along the energy conversion chain in an existing coal fired power plant and a repurposed sub- and supercritical plant are also displayed in a Sankey diagram in Fig. 7. Repurposed coal-

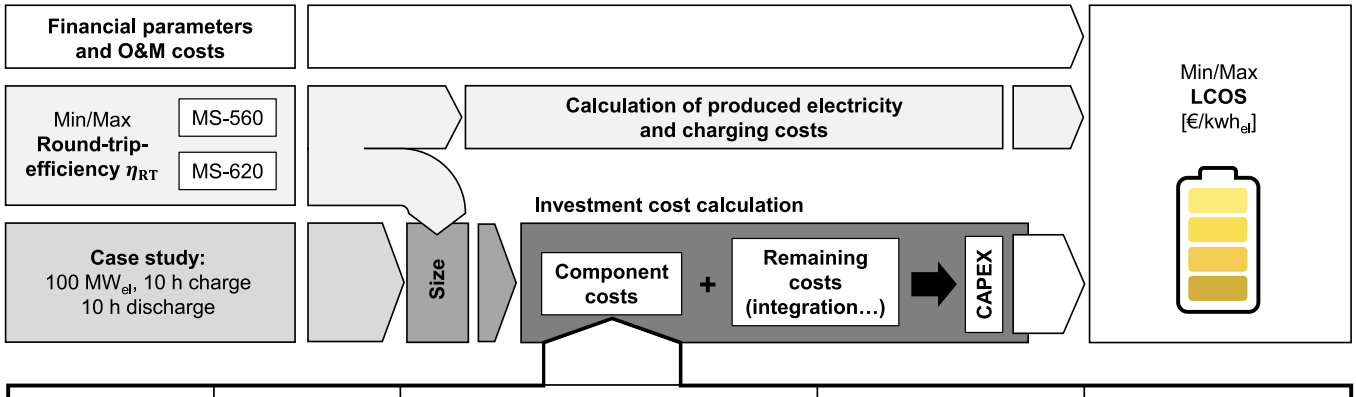

	Electric heater	Molten salt storage		Gas handling system GHS	Salt steam generator
		2T	1T		
MS-560: Subcritical plant + 560°C storage	Reference from literature	Reference from literature	Not investigated	Not required	Reference from literature
MS-620: Supercritical plant + 620°C storage	Correction factor: $CF6$: surface area	Correction factors: $CF1$: energy density $CF2$: strength	$CF3$: tank number $CF4$: surplus salt $CF5$:thermal stress	Bottom up cost analysis	Correction factors: $CF7$: surface area $CF8$: layout

Fig. 6. Overall methodology of LCOS-calculation.

Table 3
Efficiency results for existing and retrofitted coal fired power plants with sub- und supercritical steam parameters.

	Subcritical coal	MS-560	Supercritical coal	MS-620
Net efficiency coal ($\eta_{net,coal}$) [50]	27 %–37.4 %	–	38.4 %–44 %	–
Coal-fired boiler efficiency ($\eta_{SG,coal}$) / steam generator efficiency ($\eta_{SG,s}$)	80 %–90 %	100 %	90 %*	100 %
Electric heater efficiency (η_{EH})	–	98 %**	–	98 %**
Storage efficiency (η_{TES})	–	99 %***	–	99 %***
Net efficiency salt ($\eta_{net,s}$)	33.8 %–41.6 %		42.7 %–48.9 %	
Nom. round-trip-efficiency ($\eta_{RT,nom}$)	–	32.8 %–40.4 %	–	41.4 %–47.4 %
Dynamic efficiency (η_{dyn})	–	95%–100 %	–	95 %–100 %
Real round-trip-efficiency ($\eta_{RT,real}$)	–	31.2 %–40.4 %	–	39.3 %–47.4 %

* *Average value for coal fired boilers according to* [57].
** *Based on three offers from manufactures of minerally insulated resistance heaters.*
Losses include transformer losses, wire losses, losses in control electronics and heat losses.
*** *Thermal losses of a fully charged storage based on one cycle per day.*

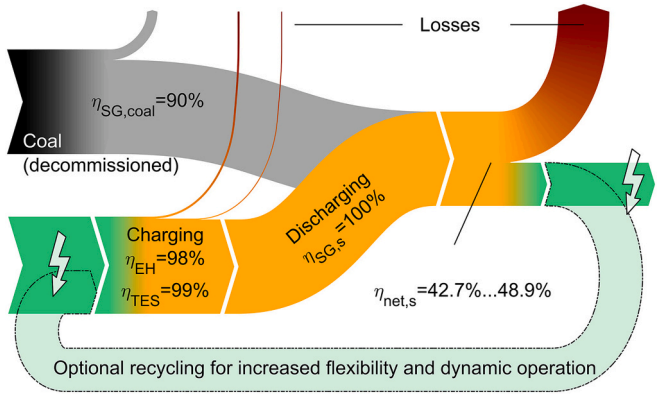

Fig. 7. Sankey diagram for an existing coal fired power plant with supercritical steam parameters (grey) as well as for a repurposed power plant with MS-620 heat storage system (colored).

fired power plants equipped with Thermal Energy Storage (TES) are likely to operate with one or two daily cycles, similar to a grid-connected battery, requiring rapid ramp-up and ramp-down rates. This dynamic operation introduces a new efficiency metric, η_{dyn}, which accounts for the power loss due to the inability of the plant to quickly adjust its output levels, especially when starting from a cold state which can take several hours to reach full capacity. Using the formula (21), the dynamic efficiency η_{dyn} can be calculated as a function of the charge and discharge duration, the nominal and the minimum load as well as the ramp rate. For common ramp rates, a charge and discharge duration of 10 h each and a nominal load of 100 MW_{el} and a minimum load of 20 MW_{el}, the real round-trip efficiency $\eta_{RT,real}$ can be up to 5 % lower (η_{dyn} = 95 % – 100 %) than the nominal round-trip efficiency, assuming that 100 % of the electricity that needs to be discarded can be 'recycled' by storing it using the electric heater.

The time required for a coal-fired power plant to reach full operational capacity is largely dependent on the performance of the boiler and steam turbine systems. In this study, the coal-fired boiler is considered to be decommissioned. Consequently, the focus is on ramping up the new molten salt steam generator, which has a comparatively low thermal mass that can be kept warm, and the turbine system. The time required for the steam turbine to reach full capacity can be considerably shorter than the time needed to heat the entire plant from a cold or warm start. Nevertheless, supercritical power plants are typically more susceptible to load fluctuations than subcritical power plants. This is largely attributed to the elevated thermal stress and differential expansion of the turbine rotor and casing during transient conditions. Consequently, the ramp-up time and the value for η_{dyn} must be assessed on a case-by-case basis. Therefore, the calculated value for the dynamic efficiency in this study requires careful consideration.

3.2. Investment costs estimation

The following section presents the results of how the correction factors introduced in the methodology section were calculated in detail. In the context of a two-tank storage system, the correction factor *CF*1 represents the temperature difference ΔT between the hot tank and the cold tank. This difference has an influence on the energy density of the storage system. Consequently, as ΔT increases, the volume of the required salt mass and also of the tank itself decreases. The correction factor *CF*2 represents the temperature dependent material strength of the hot tank $\sigma_{al,ref}$ and σ_{al}. The cost share cs_{ht} is defined in 2.2.Thus, *CF*1 and *CF*2 can be calculated as follows:

$$CF1 = \Delta T_{ref} / \Delta T \tag{25}$$

$$CF2 = cs_{ht} \cdot \sigma_{al,ref} / \sigma_{al} \tag{26}$$

The hot tank correction factors *CF*1 accounts for the change in energy density as a function of the temperature difference between hot and cold tank (see Fig. 8a). The hot tank correction factor *CF*2 represents the

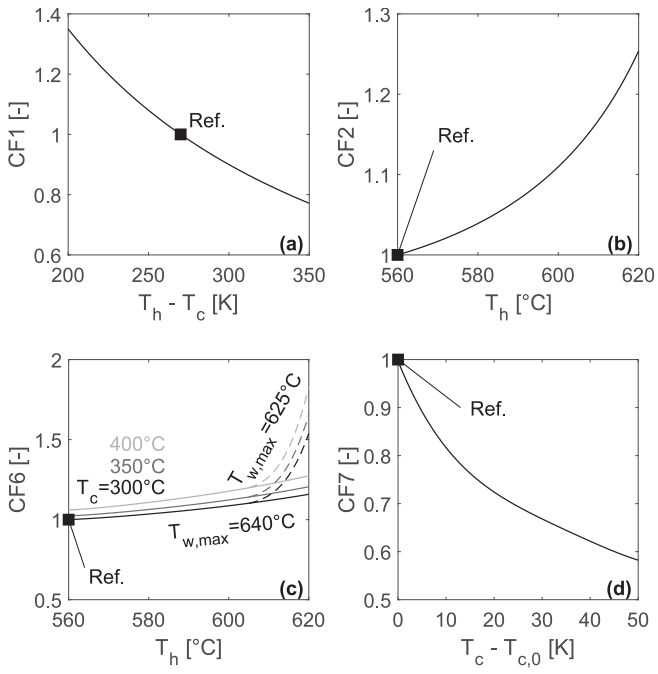

Fig. 8. Correction factors: (a) CF1 influence of energy density on specific storage costs as a function of the temperature difference between hot and cold tank. (b) CF2 influence of tank material strength decrease on specific storage costs as a function of the hot tank temperature. (c) CF6 influence of film temperature on specific electric heater costs as a function of the hot tank temperature. (d) CF7 influence of the log-mean-temperature-difference on specific steam generator costs as a function of the cold tank temperature increase.

change in tank wall thickness as a function of hot tank temperature due to tank material strength decrease. Here, σ_{al} denotes the maximum allowable stress of the material SS 347H as a function of temperature. This alloy exhibits high resistance to intergranular corrosion and demonstrates advantageous mechanical properties at elevated temperatures. The values for the yield strength and creep strength were obtained from the published data on material 1.4961, which has a composition similar to that of 1.4550 (SS 347H) [58,59]. Depending on the temperature, the lower value of the creep rupture strength and the yield strength reduced by a safety factor was selected (see Fig. 8b). The reference temperature for the maximum allowable stress $\sigma_{al,ref}$ was set at 20 K higher than the operating temperature, which was established at 580 °C.

In the single-tank configuration (no filler material), the correction factor *CF*3 represents the reduction from two tanks to only one tank, the correction factor *CF*4 represents the surplus amount of salt that is needed for the thermocline zone. In this case, it is assumed that only 95 % of the salt can be used, based on the assumption that the tank height is approximately 15 m, the non-usable salt volume of the thermocline zone has a height of 1.3 m, and the sump of the cold tank is 0.6 m. In the case of single-tank storage, the necessity for a sump is effectively eliminated since the liquid level is consistently maintained at a high level. CF5 represents the cost increase due to higher wall thickness (conservatively assumed to be 20 % higher). As these factors *CF*3, *CF*4 and *CF*5 are independent of the temperature they can directly be evaluated as follows:

$$CF3 = \left(1 - cs_{ct} - 1/2 \cdot cs_{fd}\right) = 0.83 \quad (27)$$

$$CF4 = 1/0.95 = 1.05 \quad (28)$$

$$CF5 = 1 + 0.2 \cdot cs_{ht} = 1.05 \quad (29)$$

The cost of the molten salt electric heater depends on the salt inlet temperature, on the salt outlet temperature and on the allowed wall temperature. As can be seen from Fig. 8c, the cost correction factor CF6 increases rapidly, if the maximum wall temperature $T_{w,max}$ is set to 625 °C instead of 640 °C. This considerable increase can be attributed to the fact that the required heat transfer area of the heater is directly proportional to the reciprocal of the logarithmic temperature difference. Consequently, for a hypothetical temperature difference of 0 K, the heat transfer area and, ultimately, the costs would become infinite.

Wall temperature restrictions below 640 °C are not expected at this time as Frantz et al. did not experience any gas production for wall temperatures of 633 °C [60] and Bonk et al. and Steinbrecher et al. demonstrated acceptable salt stability and low corrosion rates in solar salt with a closed gas atmosphere up to 650 °C [38,61] and the electric heater can be assumed closed. Hence, this work assumes 640 °C maximum wall temperature.

Fig. 8d shows the influence of the cold salt temperature on the cost of the steam generator. Thermodynamic data for the steam generator calculation was gathered from EBSILON®. The effect of decreasing cost with increasing cold tank temperature is due to an increased pinch point and hence a smaller required heat transfer area. In this work, the factors CF1, CF6 and CF7 were optimized. These temperature dependent variations were used cost optimization as described in 2.4. For this purpose, the cold salt temperature T_c was varied in order to minimize the $CAPEX_{comp}$.

Although a supercritical molten salt steam generator has not yet been build, a detailed cost estimation by Kelly et al. [62] showed a 10 % specific cost increase when switching from subcritical steam generation to supercritical steam generation ($CF8 = 1.1$).

The cost of the GHS was looked at with a bottom-up approach. It was based on correlations from literature shown in Table 2. The results can be seen in Fig. 9 where the additional costs per stored thermal energy is represented as a function of the design pressure of the gas system, showing a flat optimum at 35 barg and 0.13 €/kWh_{th} for the two-tank system and a flat optimum at 70 barg and 0.04 €/kWh_{th} for the single-tank system. The main cost driver with 53 % share is the pressure vessel itself. As the two-tank storage system has a greater gas volume that is exposed to recurring temperature changes, the greatest amount of inhalation and exhalation is observed in this system in comparison with the single-tank storage system. Consequently, the specific costs for the GHS are lower for the single-tank storage.

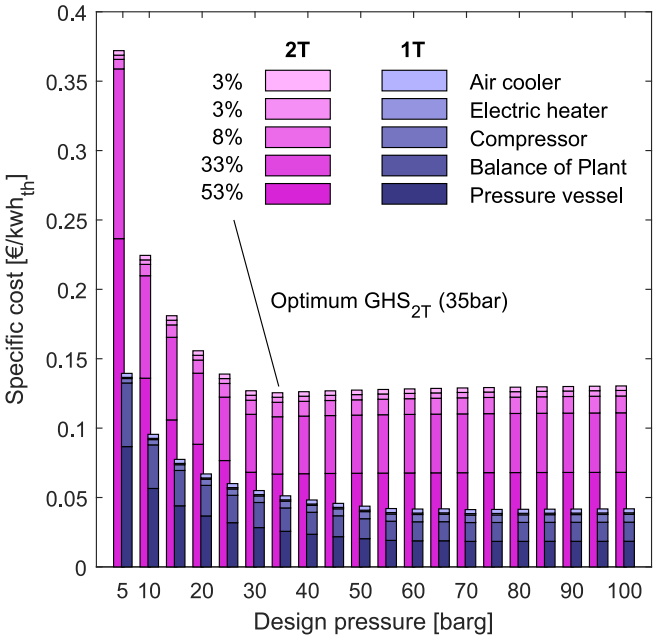

Fig. 9. Specific cost of GHS for a two-tank and single-tank system as a function of its design pressure. Optimum design pressure and component cost share is displayed. The diagram also shows at the top the cost breakdown for the optimized 2T case.

The CAPEX of retrofitting options MS-560 and MS-620 was calculated using the values presented in the following Table 4. The additional cost factors for integration and project realization are summed up and then multiplied with the total component costs $CAPEX_{comp}$.

Evaluating all correction factors for the MS-620 option in comparison to the MS-560 option results in a specific cost increase for the electric heater by 15 % from 100 €/kw_{el} to 115 €/kw_{el}. The steam

Table 4
Equipment and labour costs for CAPEX calculation of retrofitting options MS-560 and MS-620.

Equipment costs	Unit	Cost range from literature	Chosen value MS-560	Calculated value MS-620
Electric heater c_{EH}	€/kW_{el}	80 [21,63] – 140 [64]	100 [19]	115
Steam generator c_{SG}	€/kW_{th}	28 [65] - 120 [66]	46 [48]	51
Two-tank storage system c_{2T}	€/kWh_{th}		21 [48]	21*
Single-tank storage system c_{1T}	€/kWh_{th}	No data available	–	19*
Additional cost factors for integration and project realization				
Piping	–		0.19 [42]	
Electrical, instrumentation and control	–		0.13 [42]	
Structural steel and foundation	–		0.16 [42]	
Buildings and services	–		0.26 [42]	
Engineering	–		0.23 [42]	
Contingencies	–		0.3 [42]	

* *including gas handling system.*

generator is estimated to be 10 % more expensive per transferred kWh, as stated above. Finally, the specific cost of molten salt storage is estimated to be the same for the MS-560 system and the MS-620 system This is because the increase in cost due to the greater wall thickness required is offset by the decrease in cost due to the higher energy density resulting from the higher temperature difference. Consequently, while the storage will become smaller, it requires a greater wall thickness. For the single-tank storage system the specific cost of 19 €/kWh$_{th}$ are slightly lower than for the two-tank storage system. The GHS makes up less than 1 % of the specific storage costs.

In contrast, estimating the total component costs gives a different picture. Fig. 10 shows the total component cost of a storage system for a 100 MW$_{el}$ subcritical and supercritical power plant with 10 h charge and 10 h discharge time. It is worthy of note that despite the specific cost increases associated with the MS-620 system, the total cost decreases. This is attributable to the enhanced power cycle efficiencies. The costs of the electric heater decrease by approximately 6 %, those of the steam generator by approximately 9 %, and the costs of the molten salt storage by approximately 17 % for a two-tank system and by 25 % for a single-tank system. Thus, in total, the costs of the components, excluding integration costs, can be reduced by 13 % for a two-tank system and by 17 % for a single-tank system, respectively.

Table 5 lists the characteristic economical and technical values for molten salt storage and lithium-ion battery systems. The resulting energy specific system costs relate to the costs of the overall system. For a 100 MW, 10 h storage system it is in the range of 169 to 315 €/kwh$_{el}$ for a subcritical plant. For a supercritical plant with a two-tank or single-tank storage system, the energy specific cost varies between 153 and 265 €/kwh$_{el}$ and145–252 €/kWh$_{el}$, respectively. The min/max values are indicated as error bars in the figure. This range corresponds to an average reduction of 14 % for the MS-620(2T) and 18 % for the MS620 (1T) system. In comparison, the cost of lithium-ion battery systems with 10 h storage capacity and 2100 cycles lifetime per cell (4 cell replacements assumed to obtain a lifetime comparable to molten salt storage) is in the range of 613 to 861 €/kwh$_{el}$, which is a factor of three higher than the molten salt storage concepts [67] (see Fig. 11). The ramp rate of 50 %/min, achieved through preplanning and the assistance of an electric heater, indicates that the electric heater, in conjunction with a molten salt pump, requires approximately two minutes to reach full capacity when the system is preheated. This value could potentially be further optimized through the implementation of advanced control strategies, which aim to prevent overheating of the salt.

Table 5
Comparison between large scale electricity storage options MS-560, MS-620 and lithium-ion-batteries.

Value	Unit	MS-560	MS-620 (2T/ 1T)	Li-Ion [67]
Charge duration	h	10	10	unknown
Discharge duration	h	10	10	10
Discharge power	MW	100	100	100
Capacity specific cost	€/kW	1689–3149	1528–2652 / 1451–2591	3010–4054
Energy specific cost	€/kWh	169–315	153–265 / 145–252	301–405
Cycle lifetime	#	n.a.	n.a.	2100
Replacement cost after cycle lifetime	€/kWh	n.a.	n.a.	78–114
Fixed operating costs	€/kW-yr	30*	30*	6.53 - 8.03
Variable operating costs	€/MWh	1.36**	1.36**	0.5125
System lifetime	Years	30	30	10
Interest rate	–	5%	5%	5%
Round Trip Efficiency	–	31.2 % - 40.4 %	39.3 % - 47.4 %	88 %
Typical Ramp rate	1/min	5 %	5%	>100%
Ramp rate with preplanning and electric heater assistance	1/min	50 %	50 %	–

* Based on fixed operating costs for CSP (reduced by approximately 50 % heliostat field costs) [68].
** Based on variable operating costs for CSP (reduced by approximately 50 % heliostat field costs) [68].

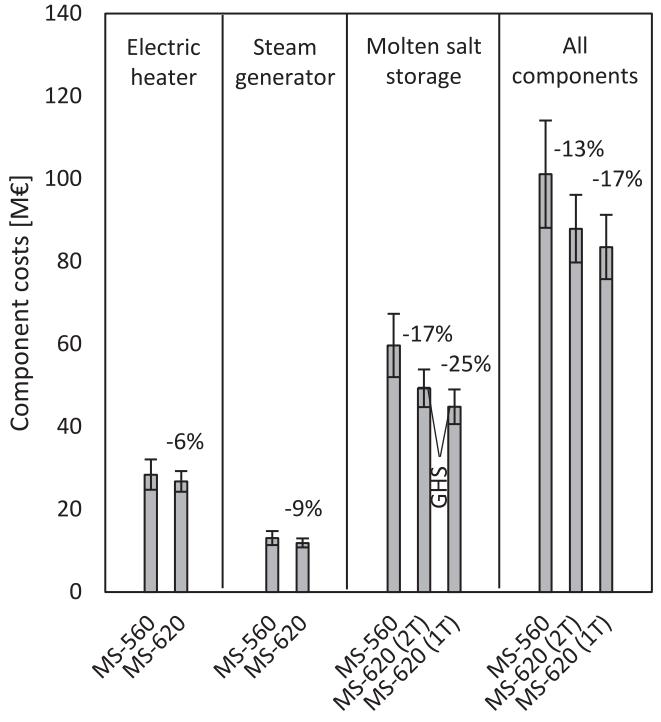

Fig. 10. Estimated average total component costs without integration costs (min/max values indicated as error-bars) for retrofitting a 100 MW$_{el}$ subcritical and supercritical power plant with a two-tank and single-tank molten salt storage system (10 h charging, 10 h discharging).

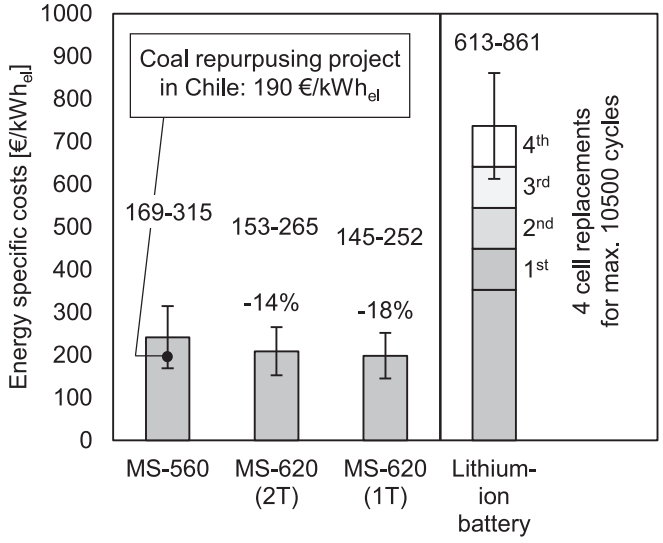

Fig. 11. Estimated average energy specific costs (min/max values indicated as error-bars) of the retrofitting option MS-560 and MS-620 with a two-tank and a single-tank storage in comparison with grid-scale lithium-ion battery systems. Black dot represents the specific costs of the planed repurposing project in Chile [25]. Energy specific costs of the lithium-ion battery system is based on [67].

3.3. Calculation of levelized cost of storage

The LCOS was calculated for the two retrofitting options MS-560 and MS-620(2T/1T) and for grid-scale lithium-ion battery systems, using the procedure described in 2.4 and the parameters described in Table 5. As the efficiency and the total CAPEX are given as a range, the LCOS is also only given as an approximate range. Fig. 12 illustrates the approximate LCOS of the retrofitting option MS-560 and MS-620(2T/1T) in comparison with grid-scale lithium-ion battery systems as a function of the charging electricity price for three different numbers of cycles per year and an operational time of 30 years. The purple-shaded area represents the anticipated levelized cost of storage (LCOS) for the retrofitting of subcritical coal power plants (MS-560). The pink-shaded area represents the anticipated LCOS for the retrofitting of supercritical power plants (MS-620). Comparing those two solutions shows that LCOS is lowest for the MS-620. Especially for a high number of cycles per year, the overlap is between the two is small. The impact of higher efficiency levels on LCOS for the MS-620 option is most pronounced when higher charging electricity prices are considered. The Angamos Power Station Project in Chile, which is planned to have a 560 °C molten salt storage, is presented as a reference [25]. A comparison of the project costs with the cost estimate reveals a sufficient degree of accuracy. The corresponding MS-560 cost estimation even yields slightly higher values for the LCOS. The grey shaded area indicates the region for the LCOS of lithium ion batteries. A comparison of the LCOS of the two options shows a clear advantage of thermal storage over lithium-ion batteries for low charging electricity prices. For 365 cycle per year lithium-ion batteries are more economical than thermal storage above approximately 50–100 €/MWh. For lower cycle numbers per year the intersection area where lithium-ion batteries are equally economical as thermal storage shifts to higher charging electricity costs. For one cycle every 4 days the option MS-620 appears to be most economical when charging electricity costs are below 125–200 €/MWh.

4. Discussion

The paper examines the potential for repurposing supercritical coal plants into flexible grid storage systems using adapted nitrate salt technology. Traditional molten salt TES systems are limited by a maximum operating temperature of 560 °C, restricting their use to subcritical steam power plants. Advanced steam power plants, however, require steam temperatures above 600 °C for optimal efficiency. This temperature gap can be addressed by using a closed gas system, preventing nitrate salt decomposition and enabling salt temperatures up to 620 °C.

A techno-economic analysis optimized the GHS design and assessed efficiency improvements by elevating TES temperatures from 560 °C to 620 °C. The study evaluated three repurposing options: MS-560, a subcritical power plant with state-of-the-art molten salt storage, and two MS-620 systems, supercritical power plants with advanced storage systems operating at 620 °C, featuring either a two-tank (MS-620(2T)) or a single-tank (MS-620(1T)) storage with a GHS.

The analysis included correction factors for component costs to assess economic viability. Key components - electric heaters, storage tanks, gas systems, and steam generators - were examined, revealing potential overall cost savings despite specific cost increases. GHS costs were negligible compared to molten salt storage costs, at 0.6 % for the two-tank system and 0.2 % for the single-tank system.

For a reference plant with a 10-h capacity, energy-specific storage costs could be reduced by 14 % and 18 % for MS-620 two-tank and single-tank systems compared to the MS-560 system. Estimated round-trip storage efficiencies were up to 40.4 % for subcritical plants and 47.4 % for supercritical plants equipped with molten salt storage.

A comparison of the LCOS for the two options MS-560 and MS-620 with state-of-the-art lithium-ion battery energy storage systems indicates that the MS-620 system offers notable efficiency enhancements over the MS-560 system and both options offer potential cost savings over lithium-ion batteries. The findings of this study underscore the potential of repurposing supercritical coal plants with adapted nitrate salt technology as a viable solution for large-scale grid energy storage. The utilization of molten salt TES in conjunction with a GHS represents a potential means of overcoming temperature-related constraints. The proposed MS-620 system demonstrates significant efficiency gains, offering a promising alternative to traditional lithium-ion battery storage solutions. Through detailed techno-economic analysis, the paper highlights the cost-effectiveness of the MS-620 system, indicating potential cost savings compared to conventional repurposing options. Moreover, the study reveals considerably lower levelized cost of storage (LCOS) of the MS560 and MS620 systems compared to lithium ion batteries when charging electricity costs are below 50 €/kWh.

5. Conclusion

This study investigates repurposing supercritical coal plants into flexible grid storage systems using adapted nitrate salt technology. Traditional molten salt TES systems are limited by a maximum operating temperature of 560 °C, restricting their use to subcritical plants. To achieve an optimal round-trip efficiency in supercritical plants,

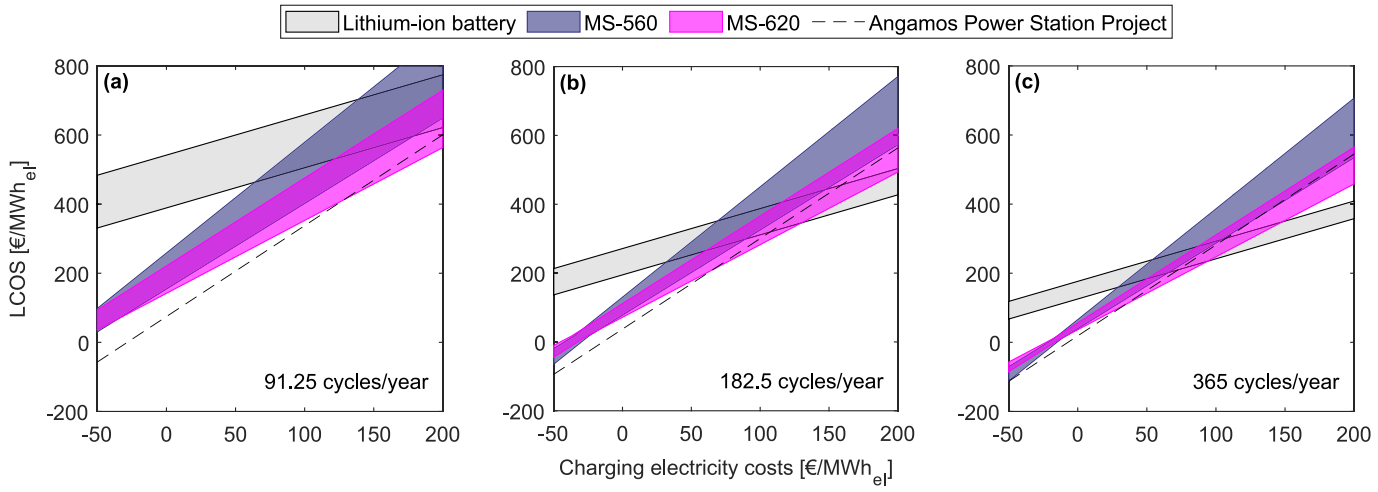

Fig. 12. Approximate LCOS of the retrofitting option MS-560 and MS-620(2T/1T) in comparison with grid-scale lithium-ion battery systems for different numbers of cycles per year (a: one cycle every four days; b: one cycle every two days; c: one cycle every day).

temperatures above 600 °C are necessary. This can be addressed by using a closed gas system, enabling salt temperatures up to 620 °C without decomposition.

A techno-economic analysis was conducted, comparing three repurposing options: MS-560 (subcritical), MS-620(2T) (supercritical with two tanks), and MS-620(1T) (supercritical with one tank). Results indicate significant efficiency improvements and cost savings with the MS-620 systems. Energy-specific storage costs could be reduced by 14 % and 18 % for the two-tank and single-tank systems, respectively, compared to the MS-560 system. Round-trip efficiencies were estimated up to 40.4 % for subcritical plants and 47.4 % for supercritical plants.

The study further demonstrates that the MS-620 system offers a promising alternative to lithium-ion batteries for large-scale energy storage. Especially for low charging electricity prices molten salt storage can be more cost effective than batteries. The research supports the viability of repurposing supercritical coal plants, contributing to the sustainable and efficient integration of renewable energy into existing infrastructure.

CRediT authorship contribution statement

Freerk Klasing: Writing – original draft, Visualization, Validation, Methodology, Investigation, Conceptualization. **Marco Prenzel:** Writing – review & editing. **Thomas Bauer:** Writing – review & editing.

Declaration of competing interest

The authors declare that they have no known competing financial interests or personal relationships that could have appeared to influence the work reported in this paper.

Data availability

The authors do not have permission to share data.

Acknowledgements

This research was funded by the German Federal Ministry for Economic Affairs and Climate Action (BMWK), (Contract No. 03EE5043).

References

[1] EU. Official Journal of the European Union (L 243). Brussels: European Union. 2021.
[2] IEA. Net Zero by 2050. A roadmap for the global energy sector. Paris: IEA; 2021.
[3] Albertus P, Manser JS, Litzelman S. Long-duration electricity storage applications, economics, and technologies. Joule 2020;4:21–32.
[4] Cahn RP. Thermal energy storage by means of reversible heat pumping. United States: Medium: X; Size; 1978. 10 2009-12-14.
[5] Mercangöz M, Hemrle J, Kaufmann L, Z'Graggen A, Ohler C. Electrothermal energy storage with transcritical CO2 cycles. Energy 2012;45:407–15.
[6] Herrmann U, Kelly B, Price H. Two-tank molten salt storage for parabolic trough solar power plants. Energy 2004;29:883–93.
[7] Gil A, Medrano M, Martorell I, Lázaro A, Dolado P, Zalba B, et al. State of the art on high temperature thermal energy storage for power generation. Part 1—concepts, materials and modellization. Renew Sust Energ Rev 2010;14:31–55.
[8] Boretti A, Castelletto S. High-temperature molten-salt thermal energy storage and advanced-ultra-supercritical power cycles. J Energy Storage 2021;42:103143.
[9] Drost MK, Antoniak ZI, Brown DR, Somasundaram S. Central Station thermal-energy storage for peak and intermediate load power-generation. Energy 1992;17:127–39.
[10] Li D, Wang J. Study of supercritical power plant integration with high temperature thermal energy storage for flexible operation. J Energy Storage 2018;20:140–52.
[11] Yong Q, Tian Y, Qian X, Li X. Retrofitting coal-fired power plants for grid energy storage by coupling with thermal energy storage. Appl Therm Eng 2022;215:119048.
[12] Wang B, Ma H, Ren S, Si F. Effects of integration mode of the molten salt heat storage system and its hot storage temperature on the flexibility of a subcritical coal-fired power plant. J Energy Storage 2023;58:106410.
[13] Li B, Cao Y, He T, Si F. Thermodynamic analysis and operation strategy optimization of coupled molten salt energy storage system for coal-fired power plant. Appl Therm Eng 2024;236:121702.
[14] Kayayan VA. Are Carnot batteries an alternative when repurposing coal power plants in Europe?. In: International renewable energy storage conference (IRES 2022). Atlantis Press; 2023. p. 3–13.
[15] Bullough C, Gatzen C, Jakiel C, Koller M, Nowi A, Zunft S. Advanced adiabatic compressed air energy storage for the Integration of wind energy. 2004.
[16] Ameen MT, Ma Z, Smallbone A, Norman R, Roskilly AP. Demonstration system of pumped heat energy storage (PHES) and its round-trip efficiency. Appl Energy 2023;333:120580.
[17] Olympios AV, McTigue JD, Farres-Antunez P, Tafone A, Romagnoli A, Li Y, et al. Progress and prospects of thermo-mechanical energy storage—a critical review. Progress in Energy 2021;3:022001.
[18] McTigue JD, Farres-Antunez P, Kavin Sundarnath J, Markides CN, White AJ. Techno-economic analysis of recuperated joule-Brayton pumped thermal energy storage. Energy Convers Manag 2022;252:115016.
[19] Trieb F, Liu P, Koll G. Thermal storage power plants (TSPP) - operation modes for flexible renewable power supply. J Energy Storage 2022;50:104282.
[20] Liu P, Trieb F. Transformation of the electricity sector with thermal storage power plants and PV – a first conceptual approach. J Energy Storage 2021;44:103444.
[21] Trevisan S, Buchbjerg B, Guedez R. Power-to-heat for the industrial sector: techno-economic assessment of a molten salt-based solution. Energy Convers Manag 2022;272:116362.
[22] Bauer T, Prenzel M, Klasing F, Franck R, Lützow J, Perrey K, et al. Ideal-typical utility infrastructure at chemical sites – definition. Operation and Defossilization Chemie Ingenieur Technik 2022;94:840–51.
[23] Hu W, Sun R, Zhang K, Liu M, Yan J. Thermoeconomic analysis and multiple parameter optimization of a combined heat and power plant based on molten salt heat storage. J Energy Storage 2023;72:108698.
[24] Marco P, Freerk K, Rüdiger F, Karen P, Juliane T, Andreas R, et al. The Potential of Thermal Energy Storage for Sustainable Energy Supply at Chemical Sites. Proceedings of the International Renewable Energy Storage Conference (IRES 2022). Atlantis Press; 2023. p. 383–400.
[25] Murray C. AES Andes looks to replace coal power plant in Chile with 560MW molten salt-based energy storage. www.energy-storage.news; 2022.
[26] Geyer M, Giuliano S. Conversion of existing coal plants into thermal storage plants. In: Cabeza LF, editor. Encyclopedia of energy storage. Oxford: Elsevier; 2022. p. 122–32.
[27] Vignarooban K, Xu X, Arvay A, Hsu K, Kannan AM. Heat transfer fluids for concentrating solar power systems – a review. Appl Energy 2015;146:383–96.
[28] Ding W, Bauer T. Progress in Research and Development of molten chloride salt Technology for Next Generation Concentrated Solar Power Plants. Engineering 2021;7:334–47.
[29] Anderson R, Bates L, Johnson E, Morris JF. Packed bed thermal energy storage: a simplified experimentally validated model. J Energy Storage 2015;4:14–23.
[30] Amy C, Pishahang M, Kelsall CC, LaPotin A, Henry A. High-temperature pumping of silicon for thermal energy grid storage. Energy 2021;233:121105.
[31] Kelsall CC, Buznitsky K, Henry A. Technoeconomic analysis of thermal energy grid storage using graphite and tin. arXiv preprint arXiv:210607624. 2021.
[32] Prieto C, Tagle-Salazar PD, Patiño D, Schallenberg-Rodriguez J, Lyons P, Cabeza LF. Use of molten salts tanks for seasonal thermal energy storage for high penetration of renewable energies in the grid. J Energy Storage 2024;86:111203.
[33] Mancini TR, Gary JA, Kolb GJ, Ho CK. Power Tower Technology Roadmap and cost reduction plan. United States: Medium: ED; Size; 2011. p. 38.
[34] Bonk A, Braun M, Sötz VA, Bauer T. Solar salt – pushing an old material for energy storage to a new limit. Appl Energy 2020;262:114535.
[35] Sötz VA, Bonk A, Steinbrecher J, Bauer T. Defined purge gas composition stabilizes molten nitrate salt - experimental prove and thermodynamic calculations. Sol Energy 2020;211:453–62.
[36] Sötz VA, Bonk A, Bauer T. With a view to elevated operating temperatures in thermal energy storage - reaction chemistry of solar salt up to 630°C. Sol Energy Mater Sol Cells 2020;212:110577.
[37] Steinbrecher J, Bonk A, Sötz VA, Bauer T. Investigation of regeneration mechanisms of aged solar salt. Materials (Basel) 2021:14.
[38] Bonk A. Thermal energy storage using solar salt at 620 °C. In: How a reactive gas atmosphere mitigates corrosion of structural materials. SolarPACES conference. Albuquerque: German Aerospace Center; 2022.
[39] Bonk A, Ding W, Hanke A, Braun M, Müller J, Klein S, et al. Effect of gas management on corrosion resistance in molten solar salt up to 620 °C: corrosion of SS316-types and SS347. Corros Sci 2024;227:111700.
[40] Kunkel S, Seeliger F, Hanke A, Bauer T, Bonk A. Demonstration of the stabilization of solar salt at 620 C with a semi-closed configuration in a 100 kg-scale. Heliyon 2023;9:e22363.
[41] Institute AP. API 650 - Welded Tanks for Oil Storage. Thirteenth ed. 2020.
[42] Perry's Chemical Engineers' Handbook. 9th Edition ed. New York: McGraw-Hill Education; 2019.
[43] Odenthal C, Klasing F, Bauer T. Investigation of the thermocline degradation in a molten salt storage tank. Albuquerque: SolarPACES conference 2022; 2022.
[44] Otto H, Naumann C, Odenthal C, Cierpka C. Unsteady inherent convective mixing in thermal-energy-storage systems during standby periods. PRX Energy 2023;2:043001.
[45] Flueckiger SM, Garimella SV. Second-law analysis of molten-salt thermal energy storage in thermoclines. Sol Energy 2012;86:1621–31.
[46] Hoffmann JF, Fasquelle T, Goetz V, Py X. A thermocline thermal energy storage system with filler materials for concentrated solar power plants: experimental data and numerical model sensitivity to different experimental tank scales. Appl Therm Eng 2016;100:753–61.

[47] Odenthal C, Klasing F, Bauer T. Parametric study of the thermocline filler concept based on exergy. J Energy Storage 2018;17:56–62.
[48] Dersch J, Paucar J, Polkas T, Schweitzer A, Stryk A. Blueprint for Molten Salt CSP Power Plant Final report of the project "CSP-Reference Power Plant" No. 0324253. 2021.
[49] Glatzmaier G. Developing a Cost Model and Methodology to Estimate Capital Costs for Thermal Energy Storage. Golden, CO (United States): National Renewable Energy Lab. (NREL); 2011. Medium: ED; Size: 1. MB.
[50] IEA. Fossil fuel-fired power generation. Paris: International Energy Agency; 2007.
[51] AD2000.. AD 2000-Regelwerk: Taschenbuch - Ausgabe 2020. Beuth Verlag GmbH; 2020.
[52] Peters MS, Timmerhaus KD, West RE. Plant design and economics for chemical Engineers. McGraw-Hill Education; 2003.
[53] Loh HP, Lyons J, White CW. Process Equipment Cost Estimation, Final Report. Morgantown, WV (United States): National Energy Technology Lab. (NETL); 2002. p. 78. Medium: ED; Size.
[54] Profaiser A, Saw W, Nathan GJ, Ingenhoven P. Bottom-up estimates of the cost of supplying high-temperature industrial process heat from intermittent renewable electricity and thermal energy storage in Australia. Processes 2022;10:1070.
[55] Energiewende Agora. Flexibility in thermal power plants – With a focus on existing coal-fired power plants. 2017.
[56] Jülch V. Comparison of electricity storage options using levelized cost of storage (LCOS) method. Appl Energy 2016;183:1594–606.
[57] DIN. Water tube boilers and auxiliary installations - part 15: Acceptance tests. DIN EN 12952-15. Berlin: Beuth-Verlag; 2004.
[58] e.V. DDIfN. EN 10028–7 - Flat products made of steels for pressure purposes - German version. Part 7: Stainless steels. 2016.
[59] Robertson Holdsworth. ECCC data sheets. European Creep Collaborative Committee; 2005.
[60] Frantz C, Buck R, Röger M, Hoffschmidt B. Experimental analysis of forced convective heat transfer of nitrate salt in a circular tube at high Reynolds numbers and temperatures. Int J Heat Mass Transf 2023;201:123563.
[61] Steinbrecher J, Hanke A, Braun M, Bauer T, Bonk A. Stabilization of solar salt at 650 °C – thermodynamics and practical implications for thermal energy storage systems. Sol Energy Mater Sol Cells 2023;258:112411.
[62] Kelly BD. Advanced Thermal Storage for Central Receivers with Supercritical Coolants. United States: Medium: ED; Size; 2010. p. 184.
[63] Guccione S, Trevisan S, Guedez R, Laumert B, Maccarini S, Traverso A. Techno-economic optimization of a hybrid PV-CSP plant with molten salt thermal energy storage and supercritical CO2 Brayton power cycle. ASME Turbo Expo 2022. Turbomachinery Technical Conference and Exposition; 2022.
[64] Li R, Guo S, Yang Y, Liu D. Optimal sizing of wind/ concentrated solar plant/ electric heater hybrid renewable energy system based on two-stage stochastic programming. Energy 2020;209:118472.
[65] Schöniger F, Thonig R, Resch G, Lilliestam J. Making the sun shine at night: comparing the cost of dispatchable concentrating solar power and photovoltaics with storage. Energy Sources B: Econ Plan Policy 2021;16:55–74.
[66] Kolb GJ. An evaluation of possible next-generation high temperature molten-salt power towers. United States: Medium: ED; Size; 2011. p. 121.
[67] Mongird K, Viswanathan V, Alam J, Vartanian C, Sprenkle V, Baxter R. Grid energy storage technology cost and performance assessment. US Department of Energy 2020;2020:98.
[68] Kolb GJ, Jones SA, Donnelly MW, Gorman D, Thomas R, Davenport R, et al. Heliostat cost reduction study. Albuquerque: Sandia National Laboratories; 2007.